Korean J. Chem. Eng., 39(3), 576-585 (2022)
DOI: 10.1007/s11814-021-0981-3

pISSN: 0256-1115
eISSN: 1975-7220

Reactive force-field simulation of the effect of heating rate on pyrolysis behavior of lignite

Fang Xu*, Qing Wang*,†, and Chengchang Wu**

*School of Energy and Power Engineering, Northeast Electric Power University, Jilin 132012, China
**Department of Power Operation, Huaneng Qinbei Power Generation Co. Ltd., Jiyuan, 454650, China
(*Received 13 August 2021 • Revised 12 October 2021 • Accepted 13 October 2021*)

Abstract−With the help of ReaxFF-MD simulations, the non-isothermal pyrolysis behavior of lignite, especially the effect of heating rate on pyrolysis products, has been investigated in detail. The results demonstrate that increasing the heating rate is very helpful for the production of tar at lower heating rates. By contrast, at relatively high heating rates, further increasing the heating rate has less effect on the distribution of pyrolysis products. Moreover, the evolution tendencies of char and tar at lower heating rates are different from those at the relatively higher heating rates, which exist as remarkable turning points in the high temperature region. This is probably because the reaction time is longer at lower heating rates, and the possibilities of condensation and further decomposition of tar are much greater at high temperatures. Additionally, the relationship between system energy and reaction mechanism was revealed. The results indicate that with the same reaction mechanism, the system energies of non-isothermal pyrolysis are approximately equal and hardly affected by the heating rate. Finally, taking 2 K/ps as an example, the secondary reaction mechanism of tar was further analyzed, and some possible secondary reaction pathways were proposed.

Keywords: Lignite, Pyrolysis, ReaxFF-MD, Heating Rate, Secondary Reaction

INTRODUCTION

Lignite accounts for approximately 13% of total coal reserves, and has huge potential in the field of energy utilization in China [1]. However, due to its high moisture content, low energy density and easy spontaneous combustion, the wide application of lignite is restricted [2,3]. Therefore, enormous attention on upgrading lignite is essential. Pyrolysis as a prospective upgrading approach can effectively overcome the defects of lignite, and the pyrolysis products (char, tar, and pyrolysis gas) are all important energy materials with high added value [4]. Furthermore, pyrolysis is considered as the basis and key of many thermal conversion processes (e.g., gasification, liquefaction and combustion), which has a great influence on the subsequent reaction processes [5,6].

Recently, lignite pyrolysis has attracted more and more interests of researchers. Extensive experiments have been conducted on the pyrolysis characteristics of lignite.

Niu et al. [7] investigated the pyrolysis mechanism of Xuandian lignite by in-situ FTIR, and analyzed the evolution trends and kinetic characteristics of main functional groups. Ye et al. [8] explored the effects of heating rate and particle size on the oxygen evolution during lignite pyrolysis. They found that high heating rate and small particle size were favorable for the migration of oxygen to tar or char. Yu et al. [9] studied the influence of volatiles reaction on the pyrolysis products. The results indicated that the volatiles reaction led to an increase in the yield of gas and coke, along with the reduction of tar yield. Lin et al. [10] investigated the structural transformation of lignite during pyrolysis using various experimental methods, and analyzed the influence of heat treatment on the main functional groups, microstructure and microcrystalline structure. However, experimental studies are not sufficient to explain the detailed reaction mechanism of lignite pyrolysis. This is because the pyrolysis process is very complicated, and involving numerous coupled chemical reaction paths [11]. Furthermore, it is still challenging to detect free radicals accurately, as they are produced in a short time under high temperature [12]. Molecular simulation is a useful approach to study the reaction mechanism of the pyrolysis process, which has the ability to supplement the shortage of experimental research [13].

As a promising computational approach, ReaxFF-MD simulation that combines molecular dynamics (MD) with reactive force field (ReaxFF) has been successfully applied to study the reaction mechanism of macromolecular complex systems [14]. Zheng et al. [15] simulated the pyrolysis dynamic characteristic of tar using ReaxFF-MD method. They found that the evolution trend of -O-$(CH_2)_n$- was closely associated with low-temperature cross-linking reactions and the increase of C_{ar}-C_{ar} played a critical role on recombination reactions at high temperature. By ReaxFF-MD simulation, Liang et al. [16] shed light on the transformation mechanism of sulfur during the hydropyrolysis process of lignite. The results indicated that the existence of H_2 was favorable for the conversation of thiophene and thioether to thiophenol/thiol, and the removal of S in the form of gas. Liu et al. [17] studied the isothermal pyrolysis behavior of polycarbonate using ReaxFF-MD simulation. They revealed the reaction pathways of typical pyrolysis products, and found random chain scission was dominant in pyrolysis of polycarbonate. Chen et al. [18] adopted ReaxFF-MD to investigate the initial spontaneous combustion mechanisms of lignite. They found that spontaneous combustion of lignite began with the hydrogen abstraction reaction of phenolic hydroxyl groups, and the removal

†To whom correspondence should be addressed.
E-mail: rlx888@126.com

of hydroxyl groups can effectively inhibit the spontaneous combustion of lignite. To our best knowledge, a large number of researches by ReaxFF-MD simulations were performed under isothermal conditions. Only a few studies were carried out using non-isothermal method [19,20], and they mainly focused on the chemical reaction in each stage of non-isothermal pyrolysis process. However, the effect of heating rate on pyrolysis behavior is obviously different at lower and higher heating rates, which needs to be further explored.

In this paper, the influence of heating rate on non-isothermal pyrolysis process was studied via ReaxFF-MD simulations. First, the effect of heating rate on the distribution of pyrolysis products, especially tar, was explored. Then, the evolution characteristics of pyrolysis products were studied by various heating rates. Additionally, the relationship between reaction system energy and pyrolysis mechanism was revealed. Finally, a low heating rate (2 K/ps) was selected to investigate the secondary reaction of tar in detail. Our work may aid in further understanding non-isothermal pyrolysis process of lignite, and it is also beneficial to high-efficiency clean utilization of lignite.

COMPUTATIONAL METHODS

1. ReaxFF Reactive Force Field

ReaxFF is an empirical reactive force field that has the ability to describe the detailed process of the formation and breakage of bonds in chemical reactions [21]. Bond order, which is the central concept of ReaxFF, can be calculated by interatomic distances. Unlike traditional force fields, the atomic connectivity in ReaxFF is determined by the bond-order formalism. The larger the bond order is, the more stable the chemical bond is. Since the parameters of ReaxFF are derived from substantial quantum mechanics (QM) based training sets and experimental data, the calculation accuracy is approximate to that of QM [22]. Energy contributions to ReaxFF consist of the terms of bonded interactions and non-bonded interactions. The energy of bonded interactions can be obtained by the complex functions of bond order, and the non-bonded interactions (van der Waals and Coulomb) are calculated by Morse and Coulomb potentials [23]. Eq. (1) presents the computational method of the total energy in the ReaxFF reactive force field:

$$E_{sytem}=E_{bond}+E_{over}+E_{under}+E_{val}+E_{pen}+E_{tors}+E_{conj}+E_{vdWaals}+E_{coulomb} \quad (1)$$

in which E_{sytem} represents the total energy of the system, E_{over} and E_{under} denote the energy contribution of the over- and under-coordinated atom, respectively. Other energy terms containing E_{val}, E_{pen}, E_{tors}, E_{conj}, $E_{vdWaals}$, and $E_{Coulomb}$ correspond to the valence angle energy, penalty energy, torsion angle energy, conjugation effects to molecular energy, van der Waals interactions and Coulomb interactions, respectively. More detailed description regarding ReaxFF can be found from the previous works of van Duin [24,25].

2. Simulation System

The Huolinhe lignite model ($C_{201}H_{195}O_{32}N_3S_1$) [26] used in this work was proposed previously by our group, and the rationality of the model was verified by the sequence of bond-cleavage. As illustrated in Fig. 1, the molecular model contains typical structural characteristics of lignite with abundant oxygen-containing functional groups and a great number of aliphatic structures [27]. The

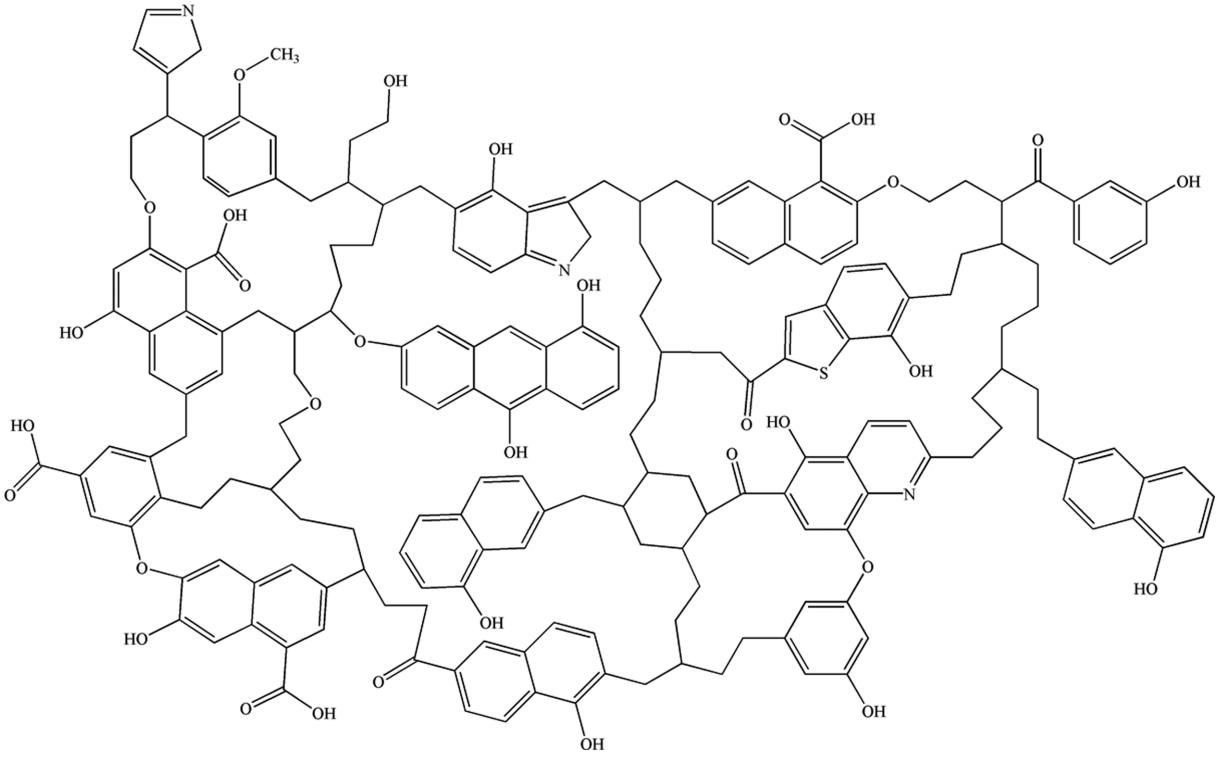

Fig. 1. Molecular structure model of Huolinhe lignite [26].

model was optimized by the calculations of molecular mechanics and molecular dynamics using Dreiding force field in Materials Studio. Zheng et al. [28] found that the molecular model was suitable for the study of pyrolysis when the number of atoms was greater than 2338. Considering the computational expense, the atomic number of macromolecular structure of lignite was set as 4320, consisting of ten optimized unimolecular models. Then, the macromolecular structure model was placed into a 81.0×81.0×81.0 $Å^3$ periodic box with a density of 0.1 g/cm^3. The lower initial density can effectively prevent stacking of significant structures, such as oxygen-containing functional groups and aromatic structures [29].

3. Simulation Details

ReaxFF-MD simulations began with the energy minimization at a lower temperature 50 K for 20 ps under NVT (constant atoms number, volume, and temperature) ensemble, and then the macromolecular model was compressed at 300 K and 10 MPa using NPT (constant atoms number, pressure, and temperature) ensemble. The density of the compressed system was 0.966 g/cm^3, which was approximate to the actual density of lignite. Then, a no-reaction MD simulation was performed at 300 K to relax the system. To prevent reaction occurrence, the parameters of C-O and O-H bonds were turned off during the relaxation simulation. Finally, a series of non-isothermal NVT-MD simulations from 300 to 3,000 K were carried out at the heating rates of 2, 10, 20, 50 and 100 K/ps, respectively, and the final temperature was needed for 10 ps. To ensure the reproducibility of the simulation results, each simulation procedure was carried out three times, and the results were the mean values of three tests. The simulation temperatures in this work were intentionally set to higher than the experimental conditions to ensure the reaction completed in an acceptable time scale (hundreds of picoseconds). In fact, higher temperatures have been widely used in previous ReaxFF-MD simulation studies [30,31], and the results were all consistent with the experimental values. The reaction temperature was regulated by Berendsen thermostat with a 100 fs damping constant, and a time step of 0.25 fs was adopted to update atom motions [11]. To analyze the product distribution, a bond-order cutoff of 0.3 was utilized to identify the molecular species. All ReaxFF-MD simulations were carried out using "reaxc" package of LAMMPS with the latest C/H/O/N/S/B force field parameters [32].

RESULTS AND DISCUSSION

1. Distribution Characteristics of Pyrolysis Products

To explore the influence of heating rate on the distribution characteristics of pyrolysis products, a series of non-isothermal pyrolysis simulations were implemented at temperatures from 300 to 3,000 K with the heating rates of 2, 10, 20, 50, and 100 K/ps, respectively, and the temperature was maintained at 3,000 K for 10 ps. On the basis of previous studies [33,34], pyrolysis products can be divided roughly into five types: inorganic gas, organic gas, light tar, heavy tar, and char. H_2O, H_2, CO, CO_2 and some inorganic small molecules are considered to be inorganic gas. Molecules with 1-4 carbon atoms are regarded as organic gas. Molecules containing 5-13 carbon atoms and 14-40 carbon atoms are regarded as light tar and heavy tar, respectively. Compounds with more than 40 carbon atoms are defined as char.

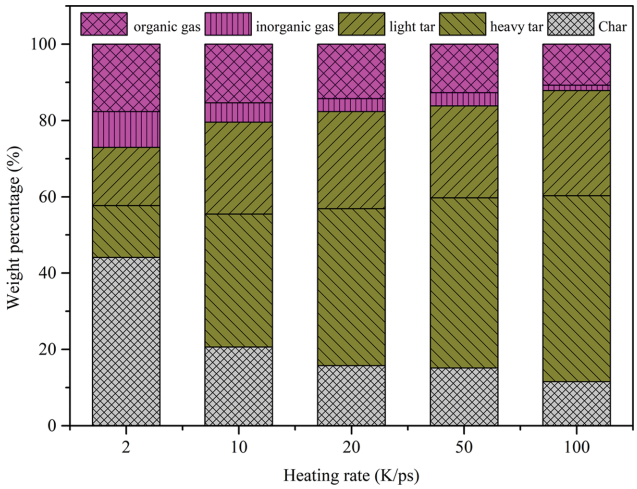

Fig. 2. Distribution of pyrolysis products at 3,000 K with five heating rates [29].

Fig. 2 shows the distribution of pyrolysis products at 3,000 K with five heating rates. The snapshots of final pyrolysis product configurations obtained by VMD are in Fig. 3. As displayed in Fig. 2, with increasing the heating rate from 2 to 100 K/ps, the yield of tar increased from 28.79% to 76.27%, along with a great reduction of char [29]. It is worthwhile mentioning that the yield of tar did not increase linearly with increasing heating rate. To quantitatively analyze the influence of heating rate on tar, Fig. 4 shows the average change of tar yield for heating rate increasing 1 K/ps in four heating intervals. As seen clearly, the tar yield increased by 3.86% for every 1 K/ps increment with the heating rate increasing from 2 to 10 K/ps. Nevertheless, when increasing heating rate from 50 to 100 K/ps, the increase of tar was only 0.095% for every 1 K/ps increment. It can be concluded that increasing the heating rate is more conducive to the formation of tar at lower heating rates. At relatively high heating rates, further increasing the heating rate had less effect on the tar production. This was mainly because the reaction time was longer at lower heating rates, and the possibility of condensation and further decomposition of tar was much greater at high temperature. Increasing the heating rate can effectively inhibit the secondary reaction of tar, leading to a notable increase of tar yield. However, at relatively high heating rates, the possibility of secondary reaction of tar was greatly reduced due to the shorter reaction time. The inhibitory effect of further increasing the heating rate on the secondary reaction of tar was obviously weakened. Therefore, further increasing the heating rate displayed much less influence on the distribution of pyrolysis products at higher heating rates.

In addition, it can be clearly seen that the yield of pyrolysis gas continued to decline with the increase of heating rate, approaching the minimum value of 12.16% at 100 K/ps. Notably, organic gas production was much more than that of inorganic gas at five heating rates. This means that organic gas was dominant in the pyrolysis gas of Huolinhe lignite. According to the analysis of pyrolysis products, C_2H_4 was the most important organic gas, which was

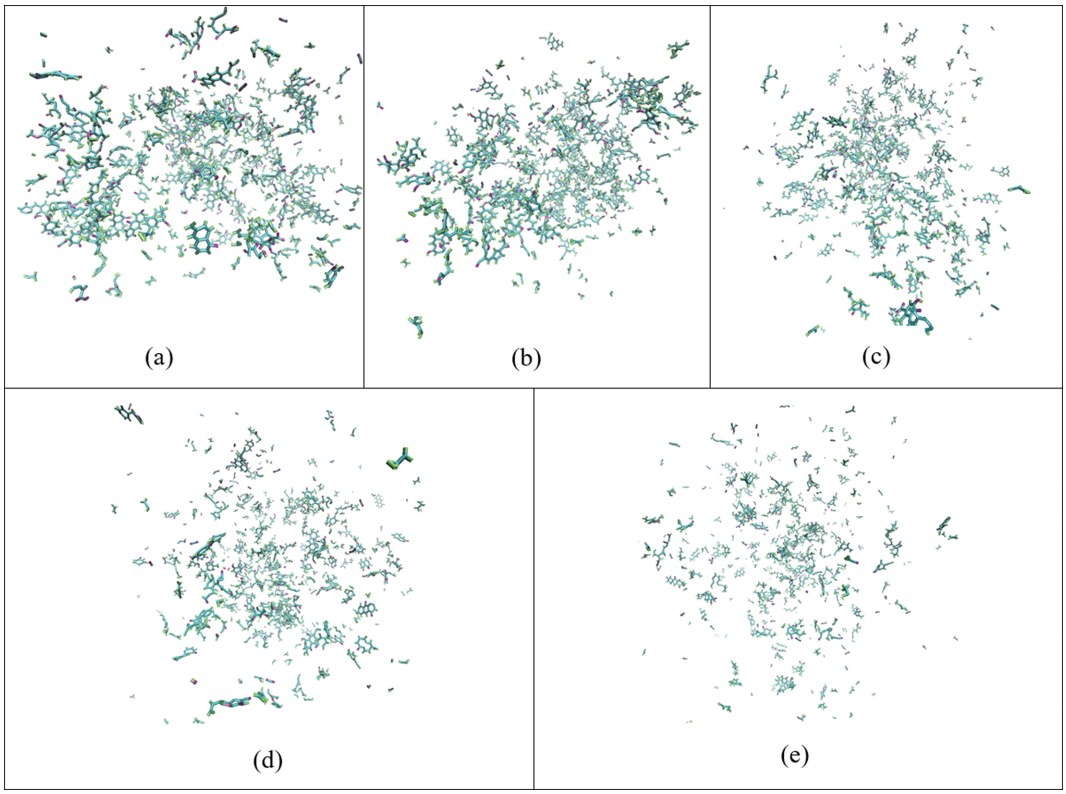

Fig. 3. Snapshots of final pyrolysis product configurations obtained by VMD: (a) Configuration at 2 K/ps, (b) configuration at 10 K/ps, (c) configuration at 20 K/ps, (d) configuration at 50 K/ps, (e) configuration at 100 K/ps.

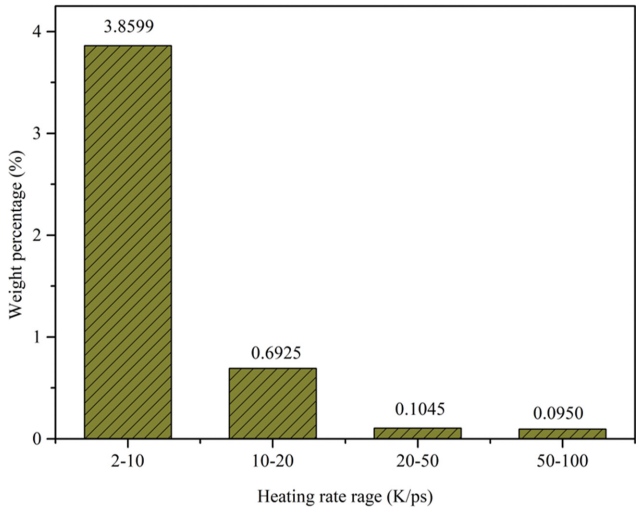

Fig. 4. Average change of tar yield for heating rate increasing 1 K/ps in four heating intervals.

mainly related to the existence of abundant methylene (C_{al}-C_{al}) in Huolinhe lignite. CO_2 and H_2O were dominant in the inorganic gas, which was due to the large amount of carboxyl and hydroxyl groups in lignite. The simulation results were in good agreement with previous studies [36].

2. Evolution Characteristics of Pyrolysis Products

Fig. 5 shows the evolution trends of char, pyrolysis gas and tar at five heating rates. As displayed in Fig. 5(a), the char production showed two different kinds of evolution trends in the whole simulation temperature range. At relatively higher heating rates (≥20 K/ps), the yield of char decreased monotonically with the increase of temperature. Nevertheless, at lower heating rates (2 and 10 K/ps), the char production decreased first and then increased with increasing temperature. Moreover, the temperatures of the turning point were both in the high temperature region. It can be speculated that the increase of char production at high temperatures was probably associated with the secondary reaction of volatiles. The average molecular weight can reflect the size of aromatic structure of char at some extent. The analysis of the change trend of average molecular weight was beneficial to investigate the secondary reaction, especially condensation reaction. To make it clear, Fig. 6 shows the average molecular weight of char as a function of temperature at different heating rates. It can be seen clearly that at the heating rates of 2 K/ps and 10 K/ps, the average molecular weight of char showed the similar variation tendencies with char yield, which decreased first and then increased, and approached the minimum values at 2,400 K and 2,800 K, respectively. In the initial stage of pyrolysis, the reduction of the average molecular weight of char can be regarded as a sign of the dissociation of the weaker bridge bonds and the decomposition of macromolecular network structures. With the further increase of temperature, the secondary reaction was dominant at high temperature. The condensation reaction between tar and char fragments resulted in the increase of aromatic structure size. Moreover, the lower the heating rate, the more suffi-

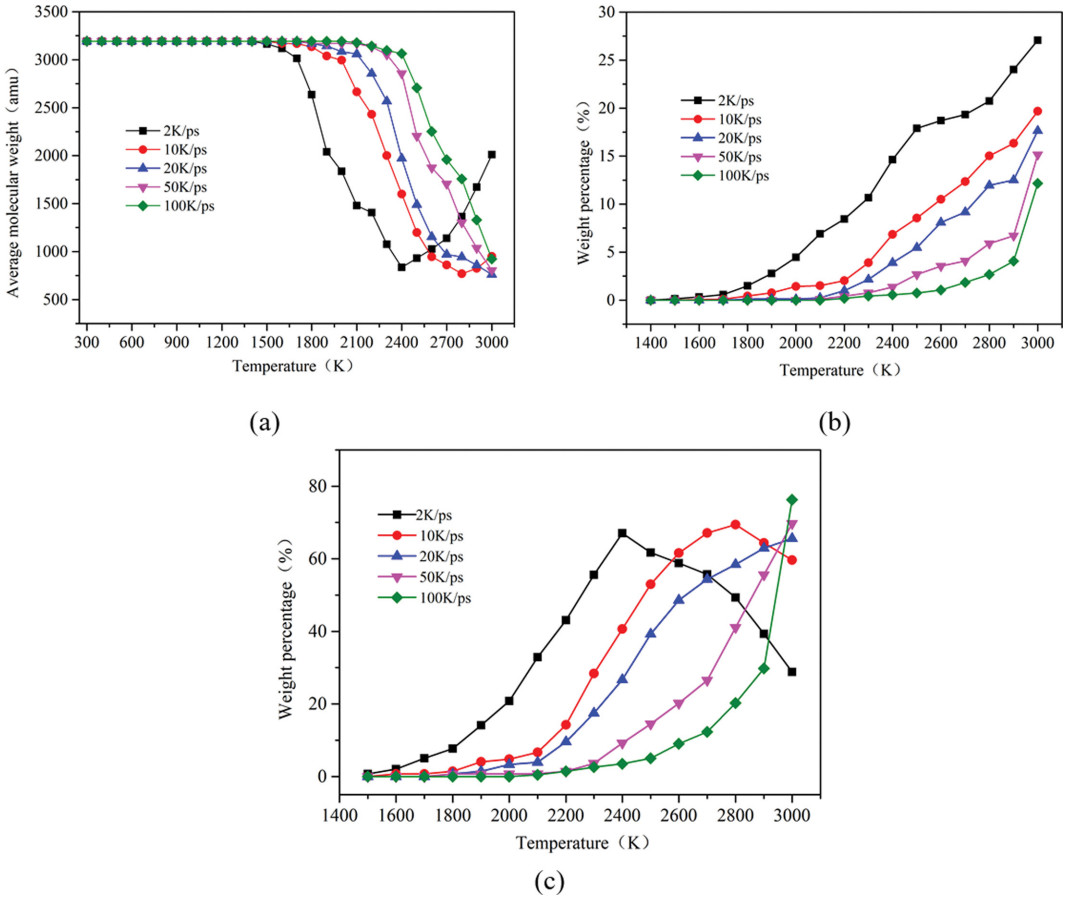

Fig. 5. Evolution trends of pyrolysis products at different heating rates: (a) char, (b) pyrolysis gas, (c) tar.

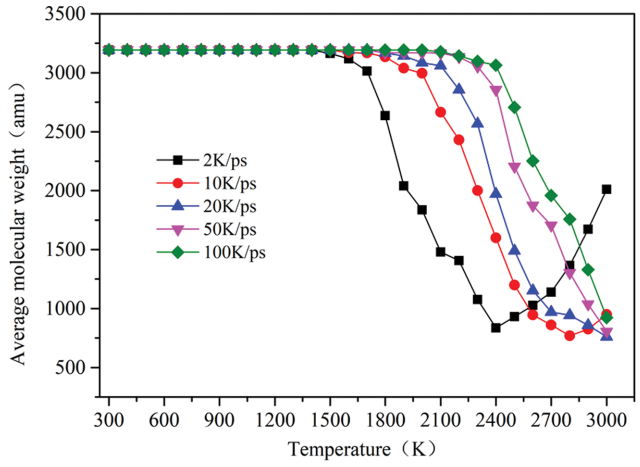

Fig. 6. Evolution trends of the average molecular weight of char at different heating rates.

cient the secondary reaction, and the larger the average molecular weight of char. However, at higher heating rates (20, 50 and 100 K/ps), the average molecular weight of char kept decreasing with increasing temperature. This was mainly because the reaction time was shortened at high heating rates, and the secondary reaction was difficult to complete in a short time. Therefore, at higher heating rates, the pyrolysis process was still dominated by the decomposition reaction, and the average molecular weight of char decreased continuously at high temperatures.

The variation trends of pyrolysis gas yield with temperature at various heating rates are presented in Fig. 5(b). Remarkably, the pyrolysis gas production and heating rate displayed an opposite variation rule at 1,800-3,000 K. The higher the heating rate, the lower the production. At lower temperatures, the primary decomposition reaction was dominant. The thermal decomposition of coal at higher heating rate was less sufficient than that at lower heating rate, which led to producing less pyrolysis gas. However, at high temperature, the secondary reaction was greatly suppressed because of the shorter reaction time at high heating rate. The possibilities of further decomposition of tar decreased obviously, resulting in the apparent decline of pyrolysis gas production. The simulation results were consistent with the studies by Tian et al. [37], who found that the pyrolysis gas production of bituminous decreased significantly with the increase of heating rate. It should be noticed that no matter what the heating rate was, an obvious increase of pyrolysis gas yield with temperature can be found in the whole simulation temperature range. This may be because the energy of the reaction system increased gradually with increasing temperature, leading to the breakage of stronger chemical bonds and the formation of more small molecules gases. Moreover, at low heating rate, the secondary reaction of tar at high temperature also led to an increase in

the yield of pyrolysis gas.

Tar is an important target product of lignite pyrolysis, which can be further processed into liquid fuel, benzene compounds, phenols and so on. Fig. 5(c) displays the evolution trends of tar yield with temperature at five heating rates. It can be seen clearly that at lower heating rates (2 and 10 K/ps), the yield of tar increased first and then decreased, and the transition temperatures were 2,400 K and 2,800 K, respectively. Moreover, at high temperatures, the decreasing trend of tar yield at 2 K/ps was more obvious than that at 10 K/ps. According to above studies of char and pyrolysis gas, the reduction of tar yield was accompanied by the increase of the weight percentage of char and pyrolysis gas at high temperature. This phenomenon suggests not only that tar can decompose into pyrolysis gas, but also generate char by condensation reaction at high temperature. Furthermore, the lower the heating rate, the more sufficient the secondary reaction. The simulation results were consistent with the previous literature [38], which found that the interaction between volatiles and char played an essential role in the distribution of pyrolysis products. Nevertheless, at higher heating rates, the tar yield increased monotonically with an increase in temperature. There was no decrease tendency of tar yield at high temperatures. This was mainly because the reaction time was shortened and the secondary reaction of tar was greatly inhibited at high heating rates.

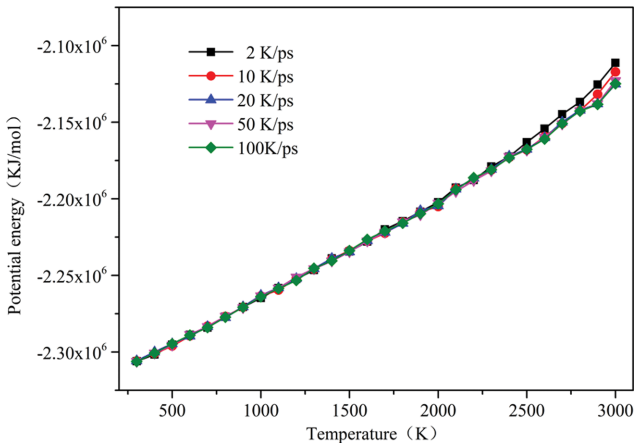

Fig. 7. Evolution trends of potential energy of non-isothermal pyrolysis at different heating rates [29].

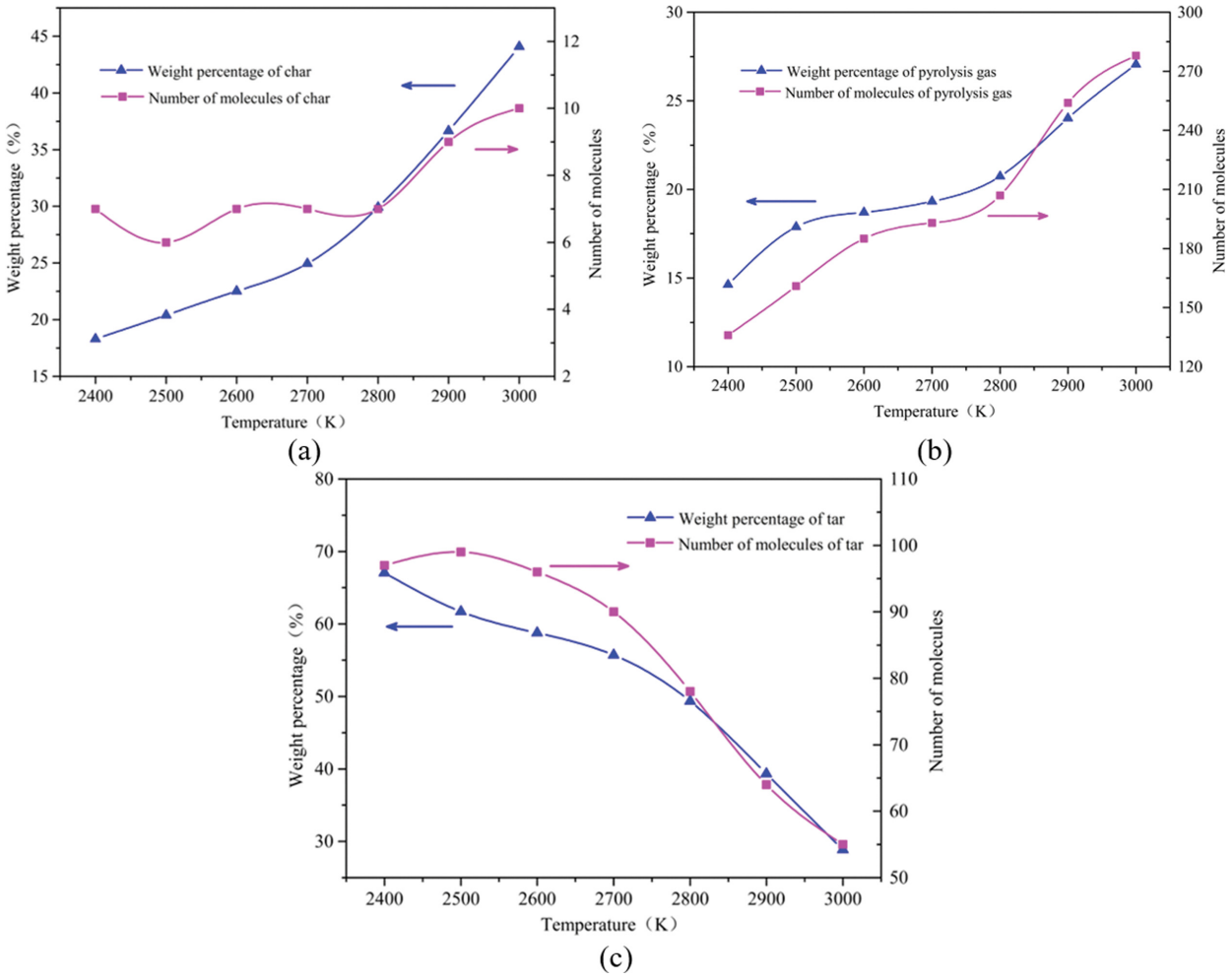

Fig. 8. Evolution trends of weight percentage and molecule number of pyrolysis products in secondary reaction process: (a) char, (b) pyrolysis gas, (c) tar.

3. Analysis of System Energy

NVT ensemble was utilized to simulate the non-isothermal pyrolysis process, and the kinetic energy of the system was considered to be nearly unchanged during the reaction process. Therefore, the evolution tendency of total system energy was almost in accord with that of potential energy. Fig. 7 shows the variation curves of potential energy with temperature at five heating rates. In the temperature range of 300-2,400 K, the potential energy of the reaction system was much similar at five heating rates [29]. As mentioned, the pyrolysis process was dominated by the primary thermal decomposition reaction of coal at lower temperature (≤2,400 K). This means that with the same reaction mechanism, the energy of the system was almost not affected by the heating rate in the non-isothermal pyrolysis process. When further increasing the temperature from 2,400 to 3,000 K, the potential energy of the system at 2 K/ps was obviously higher than that at the other four heating rates. According to Hong et al. [39], secondary reactions need more energy compared to primary decomposition reaction. It can be concluded that at the heating rate of 2 K/ps, the secondary reaction was dominant when the temperature was above 2,400 K. Above 2,800 K, the potential energy of the system at 10 K/ps was greater than that at the heating rates of 20, 50 and 100 K/ps. This indicates that at the heating rate of 10 K/ps, the reaction mechanism also changed to secondary reaction above 2,800 K. Because of the shorter reaction time at higher heating rate (20, 50 and 100 K/ps), the secondary reaction at high temperature was seriously weakened. Therefore, the decomposition reaction was still predominant at high temperature. Notably, the potential energy of the system at the heating rates of 20, 50 and 100 K/ps was approximately equal in the whole temperature range. So it can be concluded that the energy of the system was closely related to the pyrolysis reaction mechanism. With the same reaction mechanism, the energy of the system was approximately equal, which was almost not affected by the heating rate.

4. Mechanism of the Secondary Reaction

In the secondary reaction process, further decomposition of tar

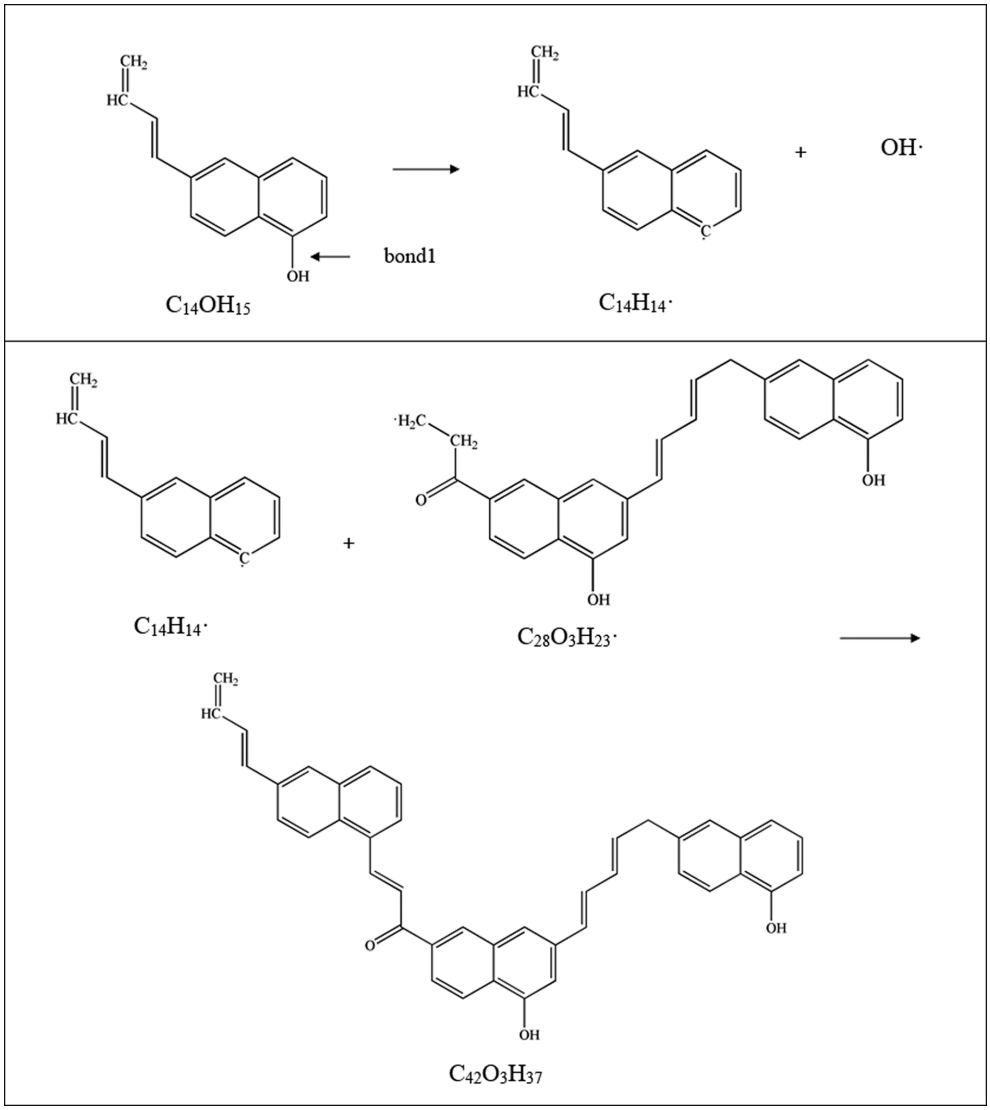

Fig. 9. Possible reaction pathways of tar fragment $C_{14}OH_{15}$.

and the condensation reactions between tar and tar, tar and char, char and char were probably taking place [40]. Therefore, the secondary reaction had a critical impact on pyrolysis products in the non-isothermal pyrolysis process. Taking the heating rate of 2 K/ps as an example, the secondary reaction stage of non-isothermal pyrolysis process was analyzed in detail. According to the above study, 2,400-3,000 K was the secondary reaction stage at 2 K/ps. Fig. 8 displays the evolution tendency of the weight percentage and molecular number of char, pyrolysis gas and tar in the temperature range of 2,400-3,000 K. As shown in Fig. 8(a), the molecule number of char increased slightly, but the obvious increase of char yield (25.79%) was found at the secondary reaction stage. It is widely known that the condensation reaction between tar and tar may lead to the increase of both the weight percentage and molecular number of char. The condensation reaction between tar and char probably resulted in an increase in the weight percentage of char, but the molecular number hardly changed. The condensation reaction between char and char gave rise to the reduction of both the yield and molecular number of char. Based on the variation trends of the yield and molecular number of char, it can be speculated that three kinds of condensation reactions may exist simultaneously in the secondary reaction process. Because of the great increase of char yield, the condensation reactions between tar and tar, char and tar were dominant.

As shown in Fig. 8(b) and 8(c), tar and pyrolysis gas demonstrated the opposite variation tendency in both the yield and molecular number. With increasing temperature, the yield and molecular number of pyrolysis gas increased significantly, while those of tar decreased continuously. Therefore, it can be concluded that in the secondary reaction stage, some tar fragments were converted into

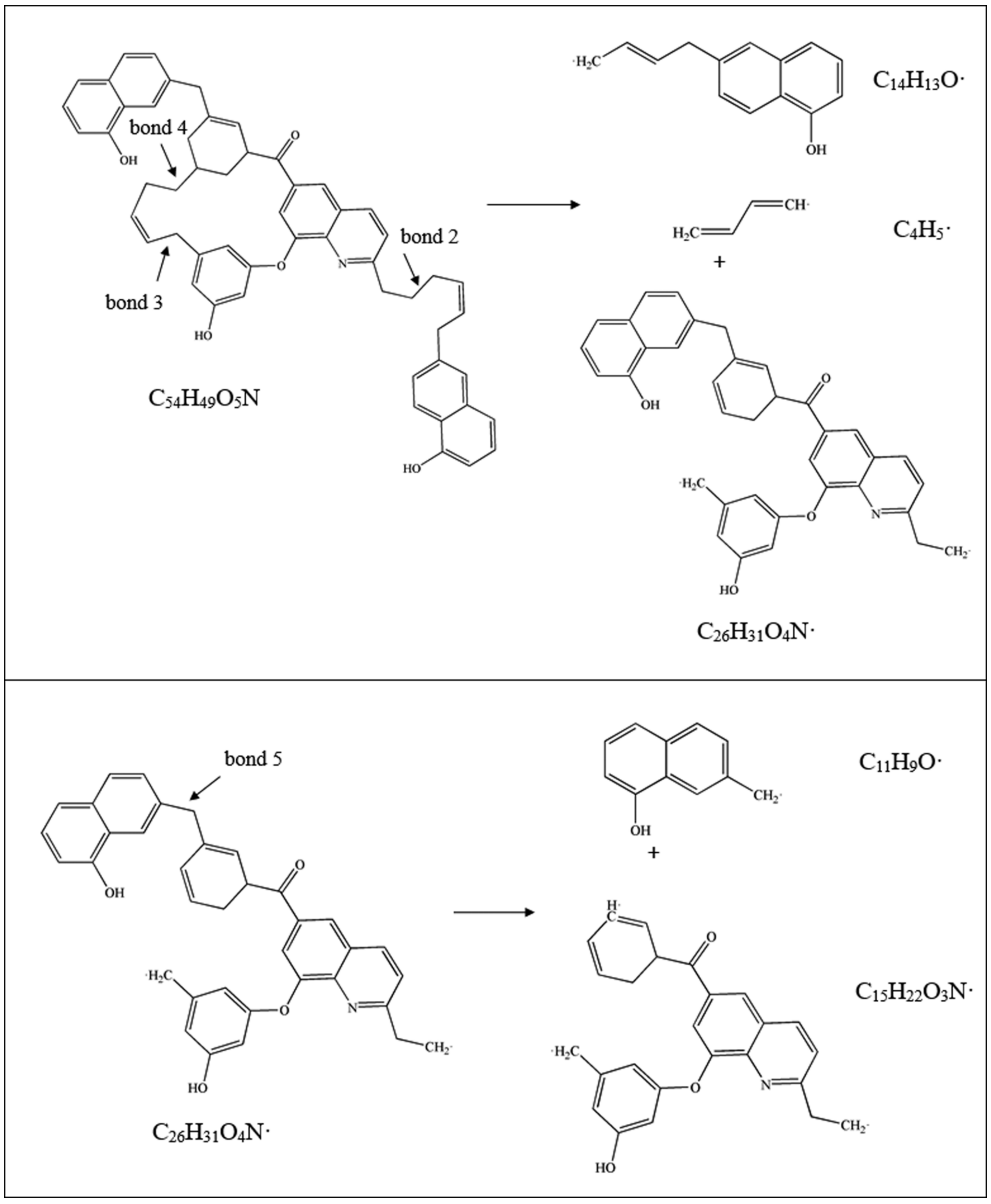

Fig. 10. Possible reaction pathways of char fragment $C_{54}H_{49}O_5N$.

char by condensation reactions, and some tar fragments were decomposed into pyrolysis gas. Meanwhile, the formation of a small part of pyrolysis gas was relevant to the condensation of aromatic structures. According to the variation of the yield of pyrolysis products, it can be known that about 67% tar was converted to char by condensation reaction, while around 33% tar was transformed into pyrolysis gas by thermal decomposition. Thus, it can be concluded that condensation reaction played a dominant role in the secondary reaction process.

With the aid of simulation trajectory and product analysis, some possible reaction paths of condensation and decomposition in the secondary reaction process can be obtained. As displayed in Fig. 9, the tar fragment $C_{14}OH_{15}$ first underwent dehydroxylation reaction, the breakage of C_{ar}-O bond (marked as bond 1) gave rise to the production of new tar fragment $C_{14}H_{14}$· and hydroxyl radical OH·. Hydroxyl radical OH· combined with hydrogen radical H· to form H_2O. Then, condensation reaction took place between active tar fragments $C_{14}H_{14}$· and $C_{28}O_3H_{23}$·, resulting in the formation of char $C_{42}O_3H_{37}$.

Fig. 10 shows the possible decomposition reaction pathways of $C_{54}H_{49}O_5N$. It can be seen clearly that the C_{al}-C_{al} bonds (marked as bond 2, 3 and 4) broke down to form heavy tar fragments $C_{14}H_{13}O$·, $C_{26}H_{31}O_4N$· and small molecular free radical C_4H_5·. Subsequently, C_4H_5· reacted with hydrogen radical H· to form organic gas C_4H_6. With increasing temperature, the cleavage of C_{ar}-O bond contributed to the further decomposition of heavy tar fragments $C_{26}H_{31}O_4N$·, which produced light tar fragment $C_{11}H_9O$· and heavy tar fragment $C_{15}H_{22}O_3N$·. In the process of pyrolysis reaction, heavy tar and light tar can be either the intermediate products or final products. There was a competitive relationship between the formation and further decomposition of tar, which largely depended on the reaction temperature.

CONCLUSIONS

ReaxFF-MD simulations were used to study the effect of heating rate on pyrolysis behavior for lignite. The results show that compared to the relatively high heating rates, further increasing the heating rate has a much greater impact on the distribution of pyrolysis products, and is more conducive to the formation of tar at lower heating rates. Moreover, the variation tendencies of char and tar at lower heating rates are different from those at the relatively higher heating rates, which is mainly caused by different reaction mechanisms. At lower heating rates, the pyrolysis process involves not only the primary decomposition reaction of coal but also the secondary reaction of tar. The decomposition reaction was always predominant in the whole reaction process at the relatively high heating rates. Furthermore, when the reaction mechanism of non-isothermal pyrolysis process was the same, the system energy was approximately equal and was hardly affected by the heating rate. The mechanism of the secondary reaction of tar was analyzed in detail at 2 K/ps, and the results suggested that condensation reaction was dominant in the secondary reaction process. Because lignite contains a large number of oxygen-containing functional groups, future work will focus on the migration mechanism of organic oxygen during pyrolysis process.

ACKNOWLEDGEMENTS

The authors gratefully acknowledge the financial support received from the National Natural Science Foundation of China (Grant No. 51676032) and Program for Changjiang Scholars and Innovative Research Team in University (No. IRT13052).

REFERENCES

1. H. H. Xin, H. Wang, W. J. Kang, C. C. Di, X. Y. Qi, X. X. Zhong, D. M. Wang and F. M. Liu, *Fuel*, **259**, 116226 (2020).
2. Y. M. Yang, J. Z. Liu, X. He, Z. H. Wang, J. H. Zhou and K. F. Cen, *Korean J. Chem. Eng.*, **34**, 1250 (2017).
3. L. Ding, Z. J. Zhou, Z. H. Dai and G. S. Yu, *Appl. Energy*, **155**, 660 (2015).
4. P. Liu, D. X. Zhang, L. L. Wang, Y. Zhou, T. Y. Pan and X. L. Lu, *Appl. Energy*, **163**, 254 (2016).
5. S. C. Liu, H. Y. Zhao, X. Y. Liu, Y. H. Li, G. F. Zhao, Y. G. Wang and M. Zeng, *Fuel*, **279**, 118485 (2020).
6. L. L. Zhu and Z. P. Zhong, *Korean J. Chem. Eng.*, **37**, 10 (2020).
7. Z. Y. Niu, G. J. Liu, H. Yin, C. C. Zhou, D. Wu, B. Yousaf and C. M. Wang, *Energy Convers. Manag.*, **124**, 180 (2016).
8. C. P. Ye, H. J. Huang, X. H. Li, W. Y. Li and J. Feng, *Fuel*, **207**, 85 (2017).
9. W. H. Yu, S. Han, Z. P. Lei, K. Zhang, J. C. Yan, Z. K. Li, H. F. Shui, S. G. Kang, Z. C. Wang, S. B. Ren and C. X. Pan, *Fuel*, **244**, 22 (2019).
10. X. C. Lin, C. H. Wang, K. Ideta, J. Miyawaki, Y. Nishiyama, Y. G. Wang, S. Yoon and I. Mochida, *Fuel*, **118**, 257 (2014).
11. J. H. Zhan, R. C. Wu, X. X. Liu, S. Q. Gao and G. W. Xu, *Fuel*, **134**, 283 (2014).
12. X. X. Li, Z. Mo, J. Liu and L. Guo, *Mol. Simul.*, **41**, 13 (2015).
13. L. Zhao, J. S. Gao and C. M. Xu, *Petrol. Sci. Technol.*, **24**, 1395 (2006).
14. G. Y. Li, J. X. Ding, H. Zhang, C. X. Hou, F. Wang, Y. Y. Li and Y. H. Liang, *Fuel*, **154**, 243 (2015).
15. M. Zheng, X. X. Li, M. J. Wang and L. Guo, *Fuel*, **253**, 910 (2019).
16. Y. H. Liang, F. Wang, H. Zhang, J. P. Wang, Y. Y. Li and G. Y. Li, *Fuel Process. Technol.*, **147**, 1 (2016).
17. Q. Liu, S. X. Liu, Y. D. Lv, P. Hu, Y. J. Huang, M. Q. Kong and G. X. Li, *Fuel*, **287**, 119484 (2021).
18. B. Chen, Z. J. Diao and H. Y. Lu, *Fuel*, **116**, 7 (2014).
19. M. Zheng, X. X. Li, F. G. Nie and L. Guo, *Energy Fuels*, **31**, 3675 (2017).
20. T. T. Zhang, X. X. Li, X. J. Qiao, M. Zheng, L. Guo, W. L. Song and W. G. Lin, *Energy Fuels*, **30**, 3140 (2016).
21. K. Chenoweth, A. C. T. van Duin and W. A. Goddard, *J. Phys. Chem. A*, **112**, 1040 (2008).
22. D. A. Newsome, D. Sengupta, H. Foroutan, M. F. Russo and A. C. T. van Duin, *J. Phys. Chem. C*, **116**, 16111 (2012).
23. T. P. Senftle, S. Hong, M. M. Islam, S. B. Kylasa, Y. X. Zheng, Y. K. Shin, C. Junkermeie, R. Engel-Herbert, M. J. Janik, H. M. Aktulga, T. Verstraelen, A. Grama and A. C. T. van Duin, *Npj Comput. Mater.*, **2**, 15011 (2016).
24. A. C. T. van Duin, S. Dasgupta, F. Lorant and W. A. Goddard, *J. Phys. Chem. A*, **105**, 9396 (2001).
25. A. C. T. Van Duin, A. Strachan, S. Stewman, Q. S. Zhang, X. Xu

and W. A. Goddard, *J. Phys. Chem. A*, **107**, 3803 (2003).
26. F. Xu, S. Pan, C. G. Liu, D. Zhao, H. Liu, Q. Wang and Y. Liu, *RSC Adv.*, **7**, 41512 (2017).
27. Z. K. Li, X. Y. Wei, H. L. Yan and Z. M. Zong, *Fuel*, **153**, 176 (2015).
28. M. Zheng, X. X. Li, F. G. Nie and L. Guo, *Mol. Simul.*, **43**, 13 (2017).
29. F. Xu, H. Liu, Q. Wang, S. Pan, D. Zhao and Y. Liu, *Fuel*, **256**, 115884 (2019).
30. T. Z. Ma, T. T. Hu, D. D. Jiang, J. L. Zhang, W. Li, Y. Han and B. Örmeci, *Korean J. Chem. Eng.*, **35**, 4 (2018).
31. M. Zheng, Z. Wang, X. X. Li, X. J. Qiao, W. L. Song and L. Guo, *Fuel*, **177**, 130 (2016).
32. F. Castro-Marcano, A. M. Kamat, M. F. Russo, A. C. van Duin and J. P. Mathews, *Combust. Flame*, **159**, 1272 (2012).
33. C. Chen, L. L. Zhao, J. F. Wang and S. C. *Lin, Ind. Eng. Chem. Res.*, **56**, 12276 (2017).
34. Y. Y. Li, G. Y. Li, H. Zhang, J. P. Wang, A. Q. Li and Y. H. Liang, *Fuel*, **193**, 331 (2017).
35. J. Akhtar and N. S. Amin, *Renew. Sust. Energ. Rev.*, **16**, 5101 (2012).
36. F. Xu, H. Liu, Q. Wang, S. Pan, D. Zhao, Q. Liu and Y. Liu, *Fuel Process. Technol.*, **195**, 106147 (2019).
37. B. Tian, Y. Y. Qiao, Y. Y. Tian and Q. Liu, *J. Anal. Appl. Pyrolysis*, **121**, 376 (2016).
38. J. H. Hu, Y. H. Si, H. P. Yang, J. G. Shao, X. H. Wang, T. Z. Lei, F. A. Agblevor and H. P. Chen, *Energy Convers. Manag.*, **152**, 229 (2017).
39. D. Hong and X. Guo, *Fuel*, **210**, 58 (2017).
40. T. J. Morgan and R. Kandiyoti, *Chem. Rev.*, **114**, 3 (2014).